J. Fluid Mech. (1999), *vol.* 398, *pp.* 225–244. Printed in the United Kingdom

Interfacial dynamics of stationary gas bubbles in flows in inclined tubes

By DANIEL P. CAVANAGH[1] AND DAVID M. ECKMANN[2]

[1]Department of Biomedical Engineering, Robert R. McCormick School of Engineering and Applied Science, Northwestern University, Evanston, IL 60208, USA

[2]Department of Anesthesia and The Institute for Medicine and Engineering, University of Pennsylvania, Philadelphia, PA 19104, USA

(Received 30 July 1998 and in revised form 9 June 1999)

We have experimentally examined the effects of bubble size ($0.4 \leqslant \lambda \leqslant 2.0$), inclination angle ($0^\circ \leqslant \alpha \leqslant 90^\circ$), and tube material on suspended gas bubbles in flows in tubes for a range of Weber ($0 \leqslant We \leqslant 3.6$), Reynolds ($0 \leqslant Re \leqslant 1200$), and Froude ($0 \leqslant Fr_\alpha \leqslant 1$) numbers. Flow rates and associated pressure differences which allow the suspension of bubbles in glass and acrylic tubes are measured. Due to contact angle hysteresis, bubbles which dry the tube wall (i.e. form a gas–solid interface) may remain suspended over a range of flows while non-drying bubbles remain stationary for a single flow rate depending on experimental conditions. Stationary bubbles increase the axial pressure gradient with larger bubbles and steeper inclination angles leading to the greatest increase in the pressure gradient. Both the suspension flow range and pressure difference modifications are strongly dependent upon gas/liquid/solid material interactions. Stronger contact forces, i.e. smaller spreading coefficients, cause dried bubbles in acrylic tubes to remain stationary over a wider range of suspension flows than bubbles in glass tubes. Bubble deformation is governed by the interaction of interfacial, contact, and flow-derived forces. This investigation reveals the importance of bubble size, tube inclination, and tube material on gas bubble suspension.

1. Introduction

The interfacial mechanics of bubbles or drops within a bulk fluid are of particular interest to investigators studying oil recovery, nuclear reactor development, and intravascular gas embolism detection and treatment. Numerous reports describing the behaviour of gas bubbles within liquids or liquid drops within liquids of different properties are found in the literature. While there are industrial applications which require the infusion of gases into liquid media in order to promote mass or heat transfer, there are also conditions under which the accidental infusion of air may disrupt the operation of a system. In cardiovascular physiology, the influx of air into blood vessels, as may occur during surgery, is a potentially fatal complication for which few definitive treatments have been devised. A significant impediment to the development of adequate therapies is the lack of a thorough understanding of the interfacial and physicochemical phenomena.

Various dimensionless parameters describing drops or bubbles in flows are commonly used to evaluate the relative contributions of the predominant mechanical forces. The first is a geometric parameter, $\lambda = a/d$, which provides a measure of

bubble size where a is the diameter of the undisturbed spherical volume of the bubble ($V_{\text{bubble}} = \pi a^3/6$) and d is the surrounding tube diameter. The Reynolds number, $Re = U_b d\rho_b/\mu_b$ (U_b, bulk fluid mean velocity; ρ_b, bulk fluid density; μ_b, bulk fluid viscosity), relates the importance of the inertial forces to the viscous forces while the Froude number, $Fr = U_b/(gd)^{1/2}$ (g, gravitational acceleration), provides a comparison of the inertial to gravitational forces. As demonstrated by Maxworthy (1991), Fr may be expressed as $Fr_\alpha = U_b/(ga\sin\alpha)^{1/2}$ (α, tube inclination angle) which accounts for tube inclination and bubble volume. The Bond number, $G = \Delta\rho g d^2/\sigma$ ($\Delta\rho$, density difference; σ, surface tension), and the capillary number, $Ca = \mu_b U_b/\sigma$, provide the relative importance of gravitational and viscous forces to surface tension forces, respectively. The Weber number, $We = \rho_b U_b^2 d/\sigma = CaRe$, is frequently utilized to present the ratio of inertial to surface tension forces. The final dimensionless parameter, $\gamma = \mu/\mu_b$, is a ratio of the bubble (or drop) viscosity to that of the bulk fluid.

In performing one of the first examinations of a long gas bubble (i.e. $\lambda \gg 1$) moving steadily with low Re through a liquid filled tube, Bretherton (1961) observed that in the vertical tube the bubble rises under the effects of gravity at rates independent of bubble size. Using the Stokes equations for low-Re flow, Reinelt (1987) performed an analysis of Bretherton's (1961) problem but for a wider range of Ca. As these investigations are for low-Re flow, they provide insight into the current investigation but cannot be used for direct correlation. Following Bretherton (1961), White & Beardmore (1962) performed a similar experimental analysis and observed significant increases in rise velocities as the tube was tilted through approximately 15° off the vertical. Zukoski (1966) analysed long-bubble ($\lambda \geqslant 1.44$) behaviour in experiments studying the effects of tube inclination ($0° \leqslant \alpha \leqslant 90°$) on bubble rise velocity. Rise velocity was found to be a maximum for $\alpha \sim 45°$ and to decrease as G decreased to $G = 1$. The author also determined that the rise velocity is independent of bubble length for bubbles of $\lambda \geqslant 1.3$.

Maneri & Zuber (1974) experimentally examined the effects of inclination, bubble volume, duct geometry, and fluid properties on the rise velocity of gas bubbles in inclined ducts. For vertical tube cases, the fluid properties were found to be unimportant as inertial forces dominate. In tubes inclined off the vertical, bubble behaviour can be described by the competing effects of bubble streamlining and a decrease in the axial buoyancy component. While no analysis is provided, Maneri & Zuber also propose that surface and viscous forces may play a major role in non-vertical situations. Through experimental and theoretical techniques, Maxworthy (1991) also recognized the possible importance of surface forces in an analysis of bubble rise under an inclined plate submerged in a liquid.

An extensive amount of research has also focused on smaller bubbles or drops whose diameters are on the same order as that of the surrounding tube ($\lambda = O(1)$). Hetsroni, Haber & Wacholder (1970) provide a numerical solution for the $Re = 0$ flow field in and around a neutrally buoyant gas bubble or liquid drop moving axially within a circular tube filled with a viscous fluid. Brenner (1970, 1971) advanced this analysis by investigating the added pressure drop due to the presence of the bubble/drop and determined that the pressure change was positive for $\gamma > 0.48$ and negative for $\gamma < 0.48$. Olbricht & Leal (1982) examined the effects of density difference between the bulk and drop phases ($G \neq 0$). Even small density differences had profound effects in that the resulting eccentric drop position caused an increase in the pressure gradient. No direct interaction between the drop phase and the tube wall is reported in that work. A major limitation of these $\lambda = O(1)$ investigations as

relates to our application is that they have focused on bubbles/drops added to flows in horizontal tubes.

A few studies do exist where the authors examined the flow field around gas bubbles that are held axially stationary in downward flows in rigid tubes. Moo-Young, Fulford & Cheyne (1971) experimentally suspended small bubbles ($0.11 \leqslant \lambda \leqslant 0.32$) in a downward liquid turbulent flow with larger bubbles requiring higher suspension flow rates. Similarly, Kojima, Akehata & Shirai (1975) investigated the behaviour of bubbles of $0.04 \leqslant \lambda \leqslant 0.2$ which were held stationary in downward turbulent flows. They found that both the relative velocity and shapes of the bubbles in the flows were similar to those observed in previous rising bubble studies, i.e. $Re_{\text{bulk}} = 0$.

Lacking in the literature is an in-depth analysis of the possible physicochemical interactions which may arise when a gas bubble is suspended in an inclined rigid tube containing a bulk flow. This is especially true for bubbles in the range of $\lambda = O(1)$ with $G \geqslant 1$. In a square channel analysis of high-Re bubbles interacting with rigid inclined Plexiglas walls, Tsao & Koch (1997) do mention that at smaller inclination angles smaller bubbles would 'stick' to the tube wall, but they provide no specific analysis. Chang *et al.* (1981) considered the contact mechanics of a gas bubble ($\lambda \sim 1$) in a water flow through a small capillary tube ($d = 0.1$ cm). Due to the use of small capillary tubes, $G \ll 1$, and although this is a critical distinction in comparison to the current work, a great deal of insight is gained from their study. The authors injected bubbles of $\lambda \sim 1$ into tube flow and observed that the pressure required to dislodge the gas bubble is greater than the pressure to lodge. They attribute this phenomenon to the contact dynamics between the three phases in that the contact line exhibits a resistance to motion which must be overcome in order to induce dislodgment.

As demonstrated above, the possible interfacial interactions associated with bubbles in tube flow may play a significant role in bubble behaviour. Therefore, a brief review of basic wetting mechanics is provided for the reader. The classical problem in wetting mechanics presents a liquid drop resting at equilibrium upon a solid horizontal substrate surrounded by a gaseous phase. At each of the two-phase boundaries, density and/or compositional differences exist which give rise to the presence of tensile stresses at the interface, i.e. interfacial tensions. It is the net effect of these interfacial stresses which determines the geometric and deformation characteristics of the three-phase system. A common indicator of this force interaction is the contact angle, ϕ, which is defined as the angle between the liquid–solid interface and the line tangent to the gas–liquid interface and emanating from the triple point. The exact angle a liquid makes when in equilibrium with a solid is directly related to the interfacial free energies per unit area of the phase interactions. Frequently, a range of stable contact angles may be observed with the endpoints of the range termed the advancing and receding contact angles, i.e. ϕ_a and ϕ_r, respectively. For example, a liquid drop resting on an inclined plate may display different endpoint contact angles. Due to the tendency of the drop to slide down the plane, it deforms in an asymmetric manner resulting in distinct contact angles at the advancing and receding edges such that $\phi_r < \phi < \phi_a$, where $\phi_a - \phi_r$ represents one common definition of contact angle hysteresis which does not take into account the actual magnitude of the contact angles. For complete reviews of basic wetting mechanics the reader is directed toward the vast amount of literature on the wetting mechanics of a liquid drop resting on a solid substrate surrounded by a gaseous phase (e.g. Marmur 1997 and Spelt, Li & Neumann 1992).

Examinations of the mechanical phenomena of static drops or bubbles adhering to non-horizontal surfaces have also been presented by Iliev (1997), Dussan V. (1985),

and Dussan V. & Chow (1983). Furthermore, the deformation and/or displacement of drops or bubbles on a rigid surface due to the motion of the surrounding fluid phase has been investigated by Dimitrakopoulous & Higdon (1997), Li & Pozrikidis (1996), Feng & Basaran (1994), Dussan V. (1987), and Durbin (1988). Many investigators cite contact angle hysteresis as the mechanism which allows drops or bubbles to remain fixed to a solid surface in the presence of external flows. While contact angle hysteresis has been the focus of numerous investigations, a complete understanding of the fundamental causes is still lacking as noted by Extrand (1998) and Extrand & Kumagai (1997). Various investigations, e.g. Extrand (1998) and Good & Koo (1979), have noted that contact angle hysteresis may be attributed to a variety of factors such as surface heterogeneity, adsorption/desorption, surface roughness, or surface deformation.

In addition to investigating bubble behaviour resulting from passing liquid flows, a number of researchers have examined the mechanics of the flow field. Fan & Tsuchiya (1990) provide an excellent review of bubble wake dynamics. For flow past a bubble, as Re is increased the flow may separate from the body with the free streamlines rejoining at some downstream point forming a closed region, i.e. the wake, containing stationary vortices. As Re is increased further, the free streamlines may not rejoin downstream resulting in an open wake thereby allowing for vortex shedding. Finally, for sufficiently high Re, the unstable and unsteady nature of the flow may produce a completely turbulent wake. Since a bubble interface is deformable, the transitioning of the surrounding flow and wake from laminar to turbulent may produce significant modifications to bubble shape and stability.

In an investigation which is relevant to the current problem, Feng & Basaran (1994) numerically examined shear flow over a cylindrical bubble pinned on a slot in a wall. At a low finite Re, they found that the flow separates from the gas–liquid interface and a recirculating eddy forms behind the bubble. As Re is further increased the eddy grows in length but its width remains contained between the solid surface and the separation point. Additionally, the investigators observe two distinct modes of bubble deformation. For low Re, simple bubble skewing or tilting in the downstream direction occurs, while for high Re, the bubble displays pure upward stretching. For the high-Re flows, the asymmetric distribution of pressure on the interface reveals low pressures at the rear which result in significant interfacial deformation tending to tilt the bubble in the downstream direction.

The present work involves a gas bubble surrounded by a liquid phase within a rigid tube with the potential for the bubble and tube to form a gas–solid interface. In situations where a gas/solid interface does form, the gas bubble is said to have 'dried' onto the solid surface and the closed line at which the three phases meet is termed the contact perimeter. The overall strength of the contact force associated with a dried bubble is determined by the length of the contact perimeter and the local force acting along it. For a gas bubble of $\lambda = O(1)$ suspended within a flow in a rigid tube at fixed inclination angle ($0^\circ \leqslant \alpha \leqslant 90^\circ$), a number of forces exist which act in an interdependent manner to govern the behaviour of the bubble and its effects on the bulk flow field. These may include buoyancy, contact, inertial, surface tension, and viscous forces. An experimental analysis of gas bubbles suspended in a viscous liquid flow through a rigid circular tube inclined at angles from the horizontal to the vertical is put forth in the present work. The relative importance of the forces listed above is explored by means of varying the governing dimensionless parameters and material properties.

This paper is divided into four sections. This Section has presented relevant back-

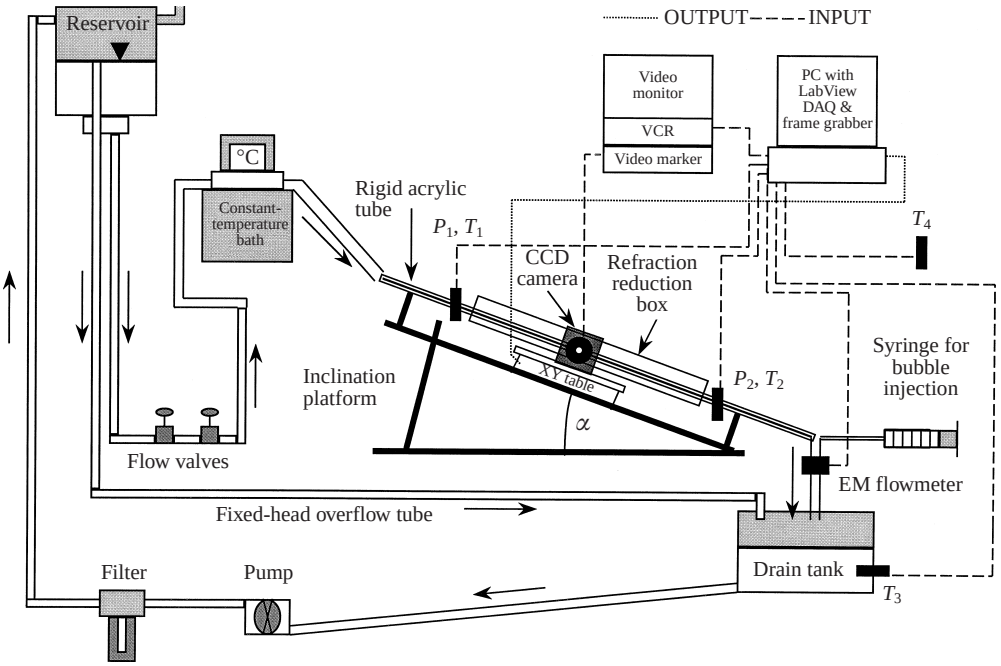

FIGURE 1. Experimental apparatus.

ground and motivation, while § 2 describes the experimental apparatus (§ 2.1), the experimental procedure (§ 2.2), and the data and image analysis techniques (§ 2.3). The experimental results and discussion, presented in § 3, comprise static bubble images (§ 3.1), static bubble geometry (§ 3.2), suspension flow ranges (§ 3.3), minimum suspension flow analysis (§ 3.4), and a pressure difference analysis (§ 3.5). At the end of the paper, we present the conclusions from the investigation (§ 4).

2. Experimental methods

2.1. *Experimental apparatus*

The experimental apparatus used in the current investigation is depicted in figure 1. The apparatus may be broken down into the following subsections for ease of discussion: test section; vibration/inclination platform; flow visualization; flow system; and the data acquisition/analysis system. The test section consists of a 64 cm length of either glass (ID = 0.57 cm) or acrylic (ID = 0.64 cm) rigid circular tubing. At both ends of the test section, specially constructed smooth bore tube couplers are used to join the test section to additional end pieces of the same tube material. These end tubes are of sufficient length in order to eliminate entrance and end effects for all flow rates examined. Machined into each of the tube couplers is a port to allow pressure and temperature measurements. Approximately 60 cm of the test section is enclosed in a glycerin filled square acrylic extruded tube in order to reduce visual distortion.

The test section is mounted orthogonally on a custom inclination platform which allows the test section to be oriented at angles ranging from 0° (horizontal) to 90° (vertical). The inclination platform is positioned on top of a 0.9 m × 1.8 m × 0.013 m steel plate resting on six air filled tubes in order to eliminate any vibrations arising

	Glass	Acrylic
Tube diameter (cm)	0.566	0.635
Static contact angle, ϕ (deg.) ($n = 15$)	43.1 $\pm$ 1.7	68.5 $\pm$ 1.2
Advancing contact angle, ϕ_a (deg.) ($n = 15$)	52.0 $\pm$ 1.8	77.0 $\pm$ 2.2
Receding contact angle, ϕ_r (deg.) ($n = 15$)	23.7 $\pm$ 1.5	48.4 $\pm$ 3.9
Contact angle hysteresis, $\phi_a - \phi_r$ (deg.) ($n = 15$)	28.3 $\pm$ 2.2	28.6 $\pm$ 5.1
Surface tension, σ (dyne cm^{-1}) ($n = 15$)	63.1 $\pm$ 3.6	63.1 $\pm$ 3.6
Spreading coefficient, S (dyne cm^{-1})	-16.9	-39.4
Bulk viscosity, μ (cP)*	0.94	0.94
Bulk density, ρ (g cm^{-3})*	0.99	0.99

* Taken from *Am. Soc. Eng. Manual*, vol. 25, 1942.

TABLE 1. Material properties at room temperature (23 $\pm$ 1 °C).

from the surrounding structure or movement of the user. To allow side view axial visualization of the bubbles, a PC controlled XY traversing table (Arrick Robotics, model XY18-MD2) with an attached CCD digital camera (Javelin, model JE-7442) is mounted onto the inclination platform. The digital image is recorded to videotape after passing through a video image marker/measurement system (Boeckeler, model VIA-150) permitting precise dimensional measurements.

In order to provide a steady laminar flow of the bulk fluid, a fixed pressure head system is utilized for the experiments. As shown in figure 1, a supply reservoir is raised 3.6 m above floor level and has a bulk fluid input, an output to the test section, an overflow output to maintain the fixed head, and an open port to maintain atmospheric pressure within the tank. Before the fluid reaches the test section, it passes through two manual flow valves and a constant-temperature bath (Brinkman Instruments, model RM6) in order to maintain the bulk fluid at 23 $\pm$ 1 °C. Directly downstream from the exit of the test section is an electromagnetic flowmeter (Carolina Medical, model 501) installed to provide flow measurements. After passing through the flowmeter, the fluid drains into the recirculation tank where it is then pumped through a polypropylene filter and returned to the supply reservoir. A differential pressure transducer (Validyne, model DP-45-20) is installed to measure the pressure difference between the machined ports in the tube couplers at the ends of the test section. The use of a differential pressure transducer accounts for the hydrostatic pressure difference which exists between the pressure ports for inclined tubes.

Due to the large volume of tap water used as the bulk fluid, the system is acknowledged as being contaminated with respect to pure water. Selected properties of the tap water have been examined for five experimental sessions providing measures of surface tension and static, advancing, and receding contact angles on glass and acrylic surfaces. The static contact angles of tap water on acrylic and glass are measured with a goniometer (Tantec) utilizing the sessile drop technique. The advancing and receding contact angles are used to determine contact angle hysteresis values and are measured using an inclining plate apparatus similar to Extrand & Kumagai (1997). These data are presented in table 1.

The primary distinctions between the glass and acrylic tube systems are the tube diameters and the strengths of the contact forces. Based on the experimental static contact angle measurements, spreading coefficients may be determined for each system. The spreading coefficient, S, is a material-dependent property and is commonly defined as $S = \sigma(\cos\phi - 1)$ where higher contact angles will result in lower spreading

	Glass tube	Acrylic tube
Effective bubble size, λ	$0.4 \leqslant \lambda \leqslant 2.0$	$0.4 \leqslant \lambda \leqslant 2.0$
Reynolds number, Re	$0 < Re < 750$	$0 < Re < 1200$
Capillary number, Ca	$0 < Ca < 0.002$	$0 < Ca < 0.003$
Weber number, We	$0 < We < 1.5$	$0 < We < 3.6$
Froude number, Fr_α	$0 < Fr_\alpha < 1.0$	$0 < Fr_\alpha < 0.8$
Bond number, G	6.1	11.9
Viscosity ratio, γ	0.019	0.019

TABLE 2. Dimensionless parameter ranges.

coefficients. For all $0^\circ < \phi < 180^\circ$, $S < 0$ with wetting ability increasing as $S \to 0$. As shown in table 1, $S_{\text{acrylic}} < S_{\text{glass}}$ indicating that the water is more likely to spread over the glass surface than the acrylic. Hence, the contact forces, or those that resist advancement of the contact line, are stronger in the air/water/acrylic system. Also, note that the calculations of contact angle hysteresis reveal similar values for each system even though the magnitudes of the contact angles in the acrylic system are larger.

2.2. *Experimental procedure*

At the start of the experiments, temperature readings are recorded to verify that the bulk fluid is at $23 \pm 1\,^\circ$C and that the axial temperature gradient in the test section is less than $0.5\,^\circ$C. With the bulk flow rate set to zero and the system flushed of all air, a bubble of known volume is introduced at either the upstream ($\alpha \leqslant 25^\circ$) or the downstream ($\alpha > 25^\circ$) end of the test section using an airtight gas syringe. The injection is performed in a rigid horizontal section of tubing to ensure that the injected air forms only one bubble. After the injection, a slight increase in the bulk flow (upstream injection) or buoyancy (downstream injection) is used to position the initially undried bubble within the test section. With the bubble inside the test section, the bulk flow rate is manipulated until the bubble has attained a stationary position. The bubble is allowed to stabilize over a two to five minute period after which the experimental analysis is initiated.

With the bubble stationary, a custom data acquisition program (LabView, National Instruments) is activated to acquire approximately 10 s of data at a rate of 50 Hz. Both the flow rate, Q_{bulk}, from the electromagnetic flowmeter and the pressure difference, ΔP_{total}, from the differential pressure transducer are recorded. For each bubble, the minimum and maximum flow rates, $Q_{\min}$ and $Q_{\max}$ respectively, which allow for suspension are acquired along with the corresponding pressure differences. Additionally, a 20 s segment of videotape of the suspended bubble is recorded for image analysis. Each individual experiment, corresponding to a specific combination of λ, α, and tube material, is carried out a minimum of three times.

2.3. *Data and image analysis*

The data acquired for each individual experiment are examined with the analysis software which calculates and records the mean and standard deviation of the flow and pressure signals. These mean values are used to determine the magnitudes of the dimensionless parameters defined in § 1 with the overall ranges presented in table 2.

Measurements of maximum bubble thickness and bubble length are extracted from the recorded two-dimensional images of the suspended bubbles using the measuring

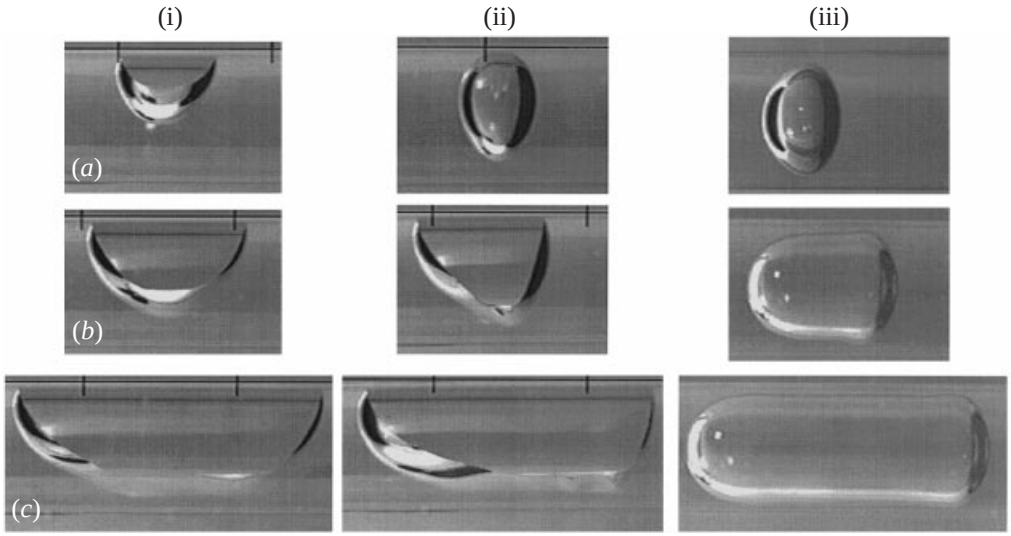

FIGURE 2. Video images of suspended bubbles in acrylic tubes. Bulk flow is from left to right. (i) $\alpha = 25°$, (ii) $\alpha = 65°$, (iii) $\alpha = 90°$. (*a*) $\lambda = 0.8$, (*b*) $\lambda = 1.1$, (*c*) $\lambda = 1.5$.

capability of the video marker system. Maximum bubble thickness, D^*, is defined as the distance from the upper tube wall to the gas/liquid interface in the core region of the bubble. Bubble length, L^*, is measured from the leading tip to the trailing edge of the bubble.

3. Results and discussion

We present below the experimentally determined suspension flows and pressures for bubbles in flows in two tube materials. Corresponding bubble geometry data are presented in order to provide physical explanations for the experimental results. For each individual experiment in the current investigation, we observed two categories into which a bubble may fall, i.e. bubbles that dry the tube wall and those that do not. While bubbles that do not dry the tube wall remain suspended for only one flow rate and pressure (Q_{bulk}, ΔP_{bulk}), those that do dry the tube wall may remain suspended over a range of flows ($Q_{\min} \leqslant Q_{\text{bulk}} \leqslant Q_{\max}$) and pressures ($\Delta P_{\min} \leqslant \Delta P_{\text{bulk}} \leqslant \Delta P_{\max}$). Flows and pressures outside the suspension ranges lead to axial translation of the dried bubble in or opposite to the direction of flow.

3.1. *Static bubble images*

Nine side view images of stationary bubbles in acrylic tubes, each from separate experiments, are presented in figure 2 in a matrix of three rows (*a–c*) and three columns (i–iii). Each row represents fixed λ while each column represents fixed α. All bubbles in this figure are held stationary under minimum suspension flow conditions with the flow directed from left to right in the images. A bubble of $\lambda = 0.8$ at $\alpha = 25°$ (figure 2 i *a*) dries the tube wall forming a distinct three-phase contact line. As the bubble volume increases (figure 2 i *b*, *c*), the larger bubbles reveal larger contact perimeters and penetrate further into the bulk flow region thereby reducing the gap width through which the bulk liquid flows. The images of bubbles of $\lambda = 1.1$ (figure 2 i *b*) and $\lambda = 1.5$ (figure 2 i *c*) reveal similar end cap profiles and similar maximum bubble thicknesses indicating that the increase in volume elongates the core region of

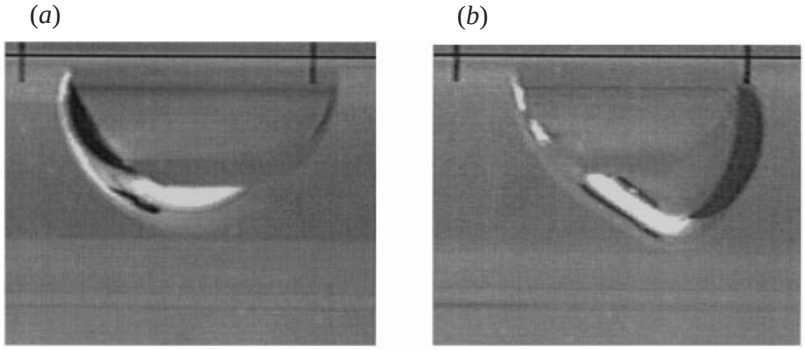

FIGURE 3. Video images of suspended bubbles of $\lambda = 1.0$ with $\alpha = 25°$. Bulk flow is from left to right. (*a*) $Q_{\min}$ flow conditions with $Re_{\min} \sim 260$, (*b*) $Q_{\max}$ flow conditions with $Re_{\max} \sim 390$.

the bubble and separates the end caps without modifying their shapes. As λ increases, the length of the dried bubble increases indicating that the water–tube interface is shrinking while the water–air interface is growing. Since these two interfaces represent extremely different boundary conditions for the bulk flow, this boundary replacement for increasing bubble size may influence the overall mechanics of bubble suspension.

For $\alpha = 65°$ and $\lambda = 0.8$ (figure 2 ii *a*), a thin liquid film remains between the bubble and the tube wall. In comparison to the same size bubble at $\alpha = 25°$ (figure 2 i *a*), the increase in α decreases the component of the buoyancy force normal to the tube wall thereby inhibiting the rupture of the thin film. However, as the bubble size increases to $\lambda = 1.1$ at $\alpha = 65°$ (figure 2 ii *b*), the buoyancy force normal to the tube wall increases producing rupture of the thin film and the bubble dries the tube wall. Further increases in λ produce drying bubbles with larger contact perimeters and elongated core regions. At $\alpha = 90°$ (figure 2 iii *a–c*), no drying is observed as all of the bubbles maintain axisymmetric positions within the vertical tube. As λ increases past $\lambda \sim 1$, the end cap geometry appears to remain fixed as the core region elongates.

Due to contact angle hysteresis, a bubble which dries a tube wall may remain stationary while undergoing a series of conformational changes due to modifications in the bulk flow rate. The endpoints ($Q_{\min}$ and $Q_{\max}$) of the range of flows for which a bubble will remain suspended correspond to distinct bubble shapes. Presented in figure 3 are images of a bubble of $\lambda = 1.0$ in an acrylic tube at $\lambda = 25°$ under $Q_{\min}$ (figure 3*a*) and $Q_{\max}$ (figure 3*b*) conditions. At $Q_{\min}$, the tendency of the bubble is to rise in the tube from right to left thereby making the left side of the bubble the leading edge and the right side the trailing edge. As Q is increased from $Q_{\min}$ to $Q_{\max}$, the axial position of the bubble remains fixed. However, the shape of the bubble has changed resulting in the left edge becoming the trailing edge and the right edge becoming the leading edge. Both the leading-edge and the trailing-edge contact angles are very similar for the two images. The deformation observed in figure 3(*b*) correlates well with the observations of Feng & Basaran (1994) where significant bulging of the downstream interface resulted from the decreased pressure in the recirculating flow region.

3.2. *Bubble geometry*

An analysis of the behaviour of the maximum thickness, D, and length, L, of the gas bubbles in the glass tubes is presented in figure 4, where the measured dimensions have been scaled with the tube diameter. Since the bubble is actually a three-dimensional

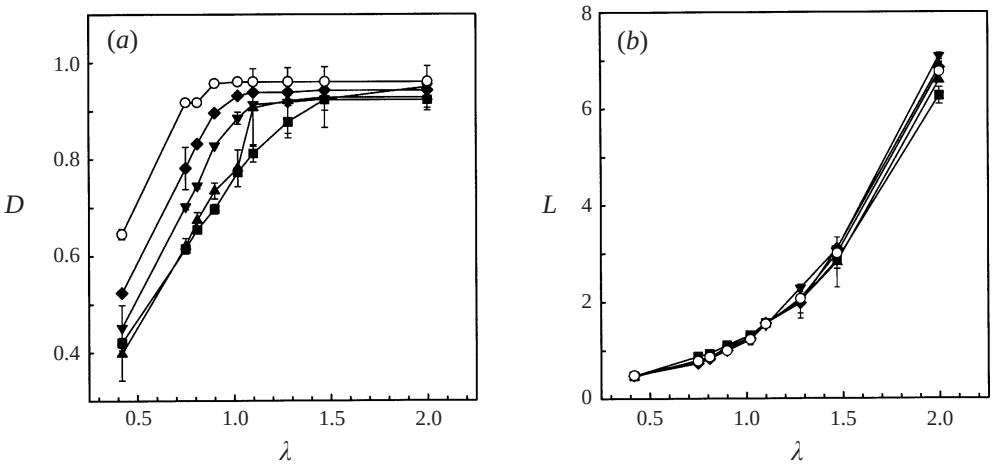

FIGURE 4. Bubble dimensions as a function of λ for bubbles in glass tubes. (*a*) Maximum bubble thickness, *D*. (*b*) Maximum bubble length, *L*. ■, $\alpha = 5°$; ▲, $\alpha = 25°$; ▼, $\alpha = 45°$; ◆, $\alpha = 65°$; ○, $\alpha = 85°$.

object, the measurements of *L* and *D* provide only a two-dimensional representation of true bubble shape. As bubble size increases, *D* plateaus in the vicinity of $\lambda \sim 1$ for all angles of inclination indicating that the cross-sectional profiles of the bubbles also level off near $\lambda \sim 1$. This behaviour of *D* also indicates that the gap width through which the bulk flow travels becomes constant for $\lambda > 1$. Since the cross-sectional profiles of the bubbles remain constant for $\lambda > 1$, any increases in volume must correspond to increasing bubble lengths. This is seen in figure 4(*b*) where as λ increases through $\lambda \sim 1$, the bubble length, *L*, increases in a cubic manner, i.e. the bubble length increases linearly with λ^3 which is proportional to V_{bubble}.

The dependence of bubble thickness on inclination angle is also apparent in figure 4(*a*) where *D* generally increases with α, indicating that the liquid gap width decreases as the bubbles occupy more and more of the tube cross-sectional area. At lower α, the buoyancy force normal to the tube wall is greater and tends to cause the bubble to flatten out along the tube wall. As α increases, this buoyancy force component is reduced thereby reducing the amount of bubble flattening. The lengths of the bubbles are observed to display a low level of dependence on α (figure 4*b*). This may appear to not correspond to the strong dependence of bubble thickness on α, but since the bubble lengths are up to seven times the tube diameter, a fractional change in the bubble thickness will have a modest effect on the bubble length.

Although the data in figure 4 are extracted from images of bubbles in glass tubes, they correlate extremely well with the images of the bubbles in acrylic tubes shown in figure 2. Examination of figure 2 shows that the maximum thickness of the bubbles also increases for increasing λ and increasing α. Furthermore, there are no significant changes in bubble length as the inclination angle is increased for fixed dimensionless bubble size, λ.

3.3. *Suspension flow ranges*

For the glass tube experiments, the suspension flow ranges, expressed as *Re*, are presented in figure 5 for all bubble sizes and four inclination angles. With the glass tube in the horizontal position (figure 5*a*) only the smaller bubbles of $\lambda \leqslant 0.9$ lead to significantly different $Re_{\max}$ and $Re_{\min}$ values. While $Re_{\min} = 0$ for all bubbles at

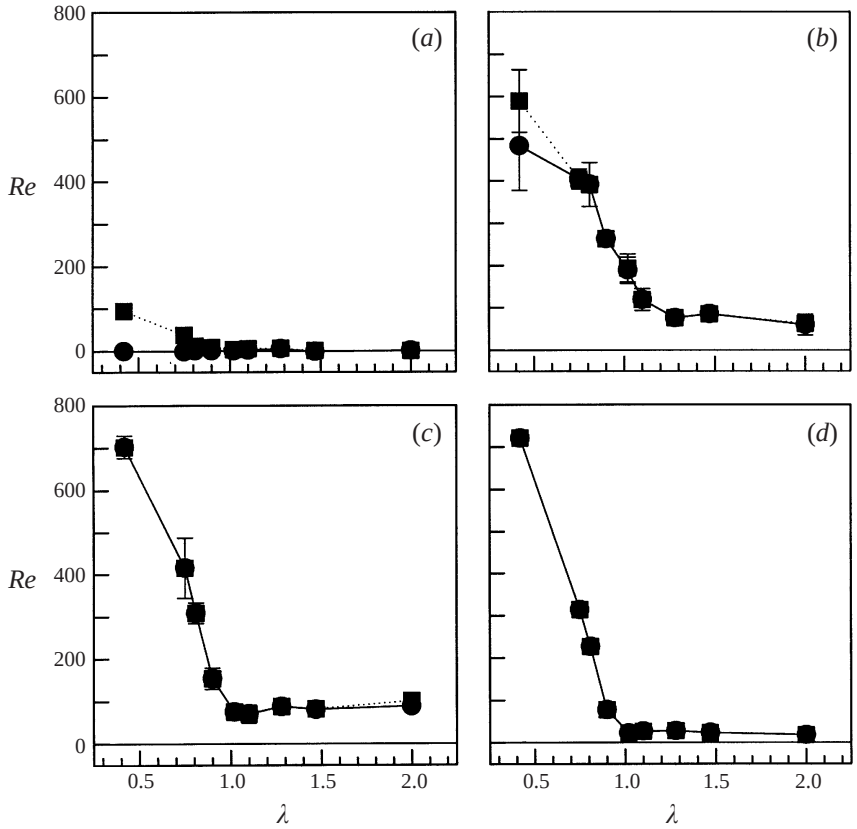

FIGURE 5. *Re* vs. λ for gas bubbles in glass tubes. ■, Re_{max}; ●, Re_{min}. (*a*) $\alpha = 0°$, (*b*) $\alpha = 25°$, (*c*) $\alpha = 65°$, (*d*) $\alpha = 90°$.

$\alpha = 0°$, the values of Re_{max} decrease with increasing bubble size. Although all of the bubbles at this angle dry the tube wall, the contact forces play a significant role only for the smaller bubbles which have smaller buoyancy forces, shorter lengths, and are thinner than the larger bubbles (figure 4). At $\alpha = 0°$, the buoyancy force has zero axial component resulting in the contact forces acting alone to resist axial motion. Due to their small surface areas and cross-sectional profiles over which the flow derived forces act, the smaller bubbles remain stationary even under flows of $Re \sim 100$. However, for increasing bubble volume, the gas/liquid surface area and the cross-sectional profile expand so that lower flow rates are required to generate adequate forces to dislodge the bubble. Subsequently, the larger bubbles ($\lambda \geqslant 1$) are easily dislodged demonstrating their high level of sensitivity to flow variations despite their larger contact perimeters.

For $\alpha > 0°$, the axial component of the buoyancy force is non-zero and, therefore, buoyancy does participate in the axial force balance on the bubble. For $\alpha = 25°$, none of the bubbles remain stationary in the absence of bulk flow (i.e. $Re = 0$) indicating that the contact forces are not sufficient to counteract the buoyancy force. The contact forces are, however, strong enough to allow the smallest bubble of $\lambda = 0.4$ to remain suspended over a distinguishable range of flows. This phenomenon disappears, however, for $\alpha = 65°$ where all bubbles remain suspended for only a single *Re* even though some of the larger bubbles ($\lambda \geqslant 1.5$) still dry the tube wall. With the tube

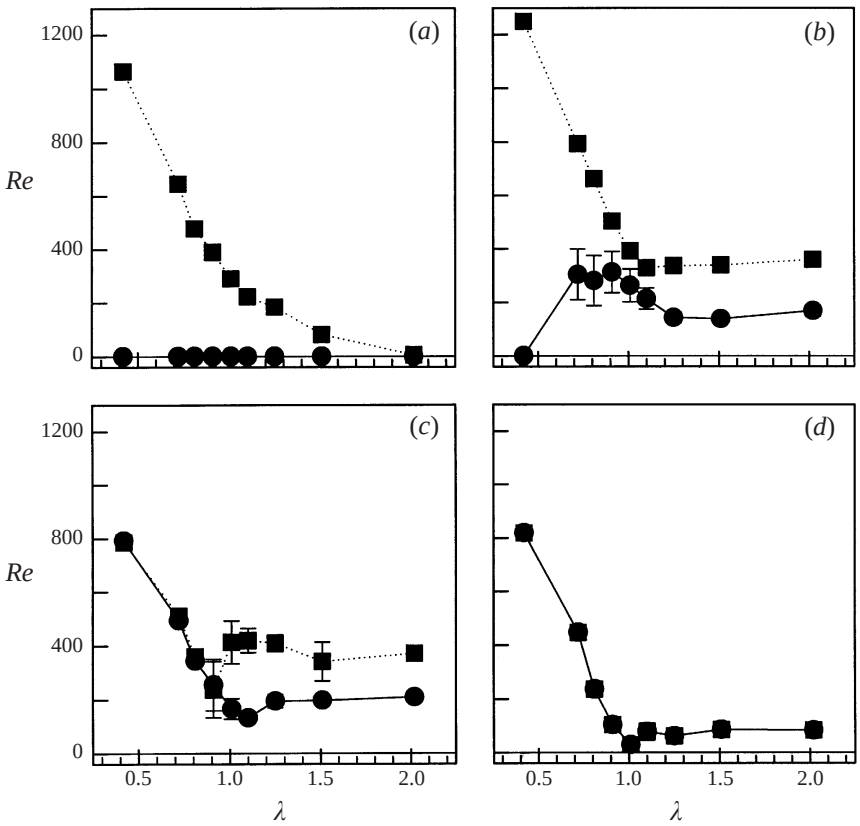

FIGURE 6. *Re* vs. λ for gas bubbles in acrylic tubes. ■, Re_{max}; ●, Re_{min}. (*a*) $\alpha = 0°$, (*b*) $\alpha = 25°$, (*c*) $\alpha = 65°$, (*d*) $\alpha = 90°$.

in the vertical position ($\alpha = 90°$), all of the bubbles take an axisymmetric position without drying the tube wall, thereby producing a situation in which $Re_{min} = Re_{max}$ for all λ. A general dependence of the suspension flows on the bubble size is found for all angles of inclination. Specifically, as λ increases the suspension flows decrease and level off in the vicinity of $\lambda \sim 1$. This correlates well with the results depicted in figure 4 and indicates a lack of dependence of the suspension flows on bubble length, L, since the bubble thickness, D, remains fixed.

The suspension flow ranges for the acrylic tube experiments are presented in figure 6. All of the bubbles in the horizontal acrylic tube are observed to dry the tube wall (figure 6*a*). While $Re_{min} = 0$ for all λ as in the glass tubes, significant differences are found in the Re_{max} values. In contrast to the glass tube results, all bubbles of $\lambda \leqslant 1.5$ display Re_{max} values which are significantly different from the corresponding Re_{min} results. In direct comparison, a bubble of $\lambda = 0.4$ in the glass tube is able to withstand the forces of a flow of $Re \sim 100$ above which the bubble is dislodged downstream. In the acrylic tube, however, a flow of $Re > 1050$ is required for dislodgment. For these similarly sized bubbles, the difference in the strength of the contact forces is responsible for the differing results. The wider suspension flow range observed in the acrylic tube is attributed to the lower spreading coefficients associated with the air/water/acrylic system (table 1). As the bubbles increase in size in the horizontal tube, we again see a transition to a region where the flow-derived forces dominate and

the larger bubbles are more sensitive to flow variations, i.e. display a more narrow suspension flow range.

In contrast to the behaviour observed in the glass tube, a bubble of $\lambda = 0.4$ at $\alpha = 25^\circ$ is able to remain dried and stationary on the acrylic tube wall even under zero flow conditions due to stronger contact forces (figure 6*b*). Also for this bubble, $Re_{\max}$ is found to be higher than was observed at $\alpha = 0^\circ$. This may be explained by the fact that at this non-zero inclination angle, the maximum flow allowable without inducing translation has to generate viscous and inertial forces which are on the verge of overcoming the buoyancy and motion-resisting contact forces. In the horizontal tube, the flow only has to overcome the contact forces to dislodge the bubble. As the bubble increases in size ($\lambda > 0.4$), the increased buoyancy force exceeds the contact forces and causes the bubble to rise in the tube, thus requiring at least minimum counterflows, $Re_{\min}$, to suspend the bubbles. There exist distinct flow ranges for which all bubbles of $\lambda > 0.4$ remain suspended due to the bubbles drying the tube as shown in figures 2 and 3.

As α is further increased to 65° (figure 6*c*), bubbles which both do not dry the wall ($\lambda < 1$) and do ($\lambda \geqslant 1$) are observed. Unlike what occurs in glass tubes, if a bubble in an acrylic tube does dry the tube wall, a distinct suspension flow range generally exists due to the stronger contact forces. At $\alpha = 65^\circ$, the buoyancy force component directed normal to the tube wall is reduced. It is this force which will play a major role in determining whether a bubble is able to rupture the thin liquid film observed between the bubble and the wall. Since α is fixed in this case, it is the changing bubble volume which is governing whether or not drying occurs as was seen in the video images shown in figure 2. Finally, similar to the bubble behaviour observed in glass tubes, non-drying bubbles attain axisymmetric positions within vertical acrylic tubes and remain suspended for only a single flow rate (figure 6*d*).

3.4. *Minimum suspension flows*

Further attention is given to the minimum suspension flows determined for bubbles in both tube types for the range of inclination angles and bubble sizes. Due to the fact that most prior investigations involving buoyancy-affected bubbles have been carried out in stagnant bulk liquids with bubble rise velocity being the commonly reported parameter, we present here a qualitative comparison between our measurements of suspension flow rates and the previously reported bubble rise velocities. For this analysis, flow rates have been scaled as $Fr_{\alpha,\min}$ which is a dimensionless velocity term providing insight into the balance of inertial and buoyancy forces.

Figure 7 displays $Fr_{\alpha,\min}$ as a function of bubble size for the glass and acrylic tube experiments. In both tube materials for all α note that as λ passes through $\lambda \sim 1$ the suspension flow values tend toward a fixed value. As shown in figures 2 and 4, as λ passes through $\lambda \sim 1$, the cross-sectional profile of the bubble remains fixed while the bubble length increases indicating an increase in the gas/liquid interfacial area. Since the magnitude of the viscous forces is directly related to the interfacial area, the observed insensitivity of the required suspension flow to bubble volume demonstrates the minor role the viscous forces play in the overall force balance on these larger bubbles. Because the cross-sectional profile of the bubble does not change greatly for $\lambda \geqslant 1$, the inertial forces remain relatively fixed and play the dominant role among the flow-derived forces. This result is in good agreement with the studies of Bretherton (1961), White & Beardmore (1962), and Zukoski (1966) who all determined that the rise velocities of large bubbles ($\lambda \geqslant 1.4$) are independent of bubble length. For all λ and α, $Fr_{\alpha,\min} < 1$ indicating that buoyancy forces dominate the inertial forces

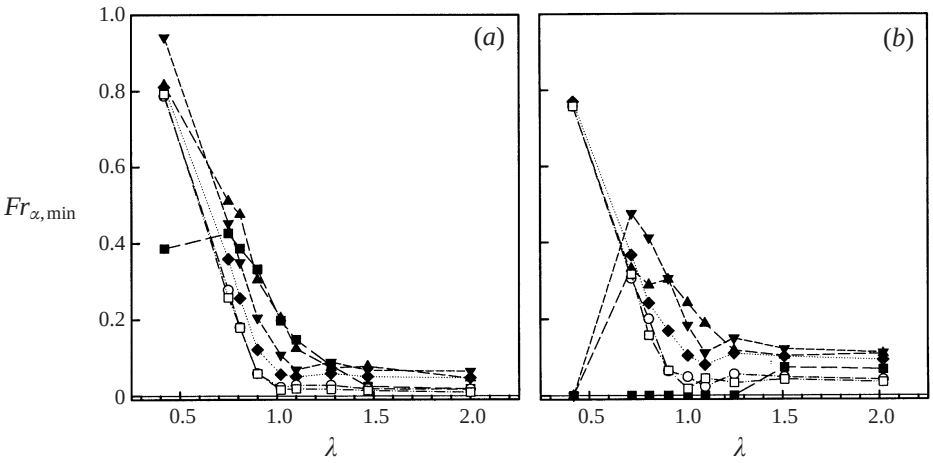

FIGURE 7. $Fr_{\alpha,\min}$ vs. λ for bubbles in (*a*) glass and (*b*) acrylic tubes. ■, $\alpha = 5°$; ▲, $\alpha = 25°$; ▼, $\alpha = 45°$; ◆, $\alpha = 65°$; ○, $\alpha = 85°$; □, $\alpha = 90°$.

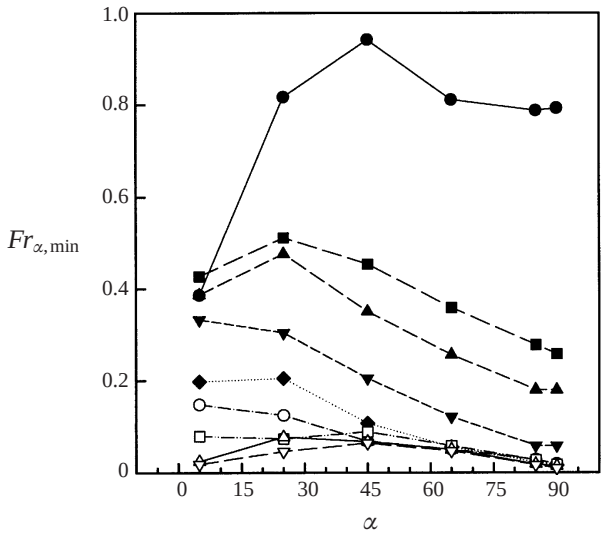

FIGURE 8. $Fr_{\alpha,\min}$ vs. α for bubbles in glass tubes. ●, $\lambda = 0.4$; ■, $\lambda = 0.75$; ▲, $\lambda = 0.8$; ▼, $\lambda = 0.9$; ◆, $\lambda = 1.0$; ○, $\lambda = 1.1$; □, $\lambda = 1.3$; △, $\lambda = 1.5$; ▽, $\lambda = 2.0$.

especially for $\lambda \geqslant 1.25$, where $Fr_{\alpha,\min} \leqslant 0.1$ for both tube materials and all α. Also, note that the $Fr_{\alpha,\min}$ values for the larger bubbles in the acrylic tube are slightly higher than those for the glass tube. This apparent discrepancy may be explained simply by the differing tube diameters. Although we are using a dimensionless analysis, the respective Bond numbers for the two systems are different with $G_{\text{glass}} \sim 0.5 G_{\text{acrylic}}$. Thus buoyancy forces are more prominent in the acrylic system thereby mandating higher suspension flows.

Figure 8 displays $Fr_{\alpha,\min}$ as a function of the inclination angle for the glass tube experiments. The observed dependence of $Fr_{\alpha,\min}$ on α for bubbles of $\lambda \geqslant 1.3$ is in agreement with the results of Zukoski (1966) and White & Beardmore (1962). While Zukoski (1966) observed that the rise velocities of large bubbles ($\lambda > 1.4$) peaked

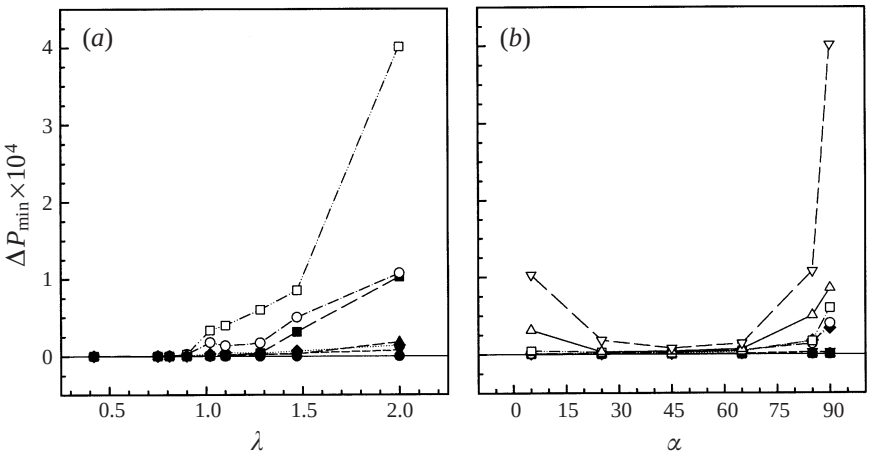

FIGURE 9. $\Delta P_{\min}$ for suspended bubbles in glass tubes. (*a*) $\Delta P_{\min}$ vs. λ: ●, $\alpha = 0°$; ■, $\alpha = 5°$; ▲, $\alpha = 25°$; ▼, $\alpha = 45°$; ◆, $\alpha = 65°$; ○, $\alpha = 85°$; □, $\alpha = 90°$. (*b*) $\Delta P_{\min}$ vs. α: ●, $\lambda = 0.4$; ■, $\lambda = 0.75$; ▲, $\lambda = 0.8$; ▼, $\lambda = 0.9$; ◆, $\lambda = 1.0$; ○, $\lambda = 1.1$; □, $\lambda = 1.3$; △, $\lambda = 1.5$; ▽, $\lambda = 2.0$.

in the vicinity of $\alpha \sim 45°$, White & Beardmore (1962) found significant increases in rise velocity as α decreased from 90° to 75°. For bubble rise under inclined plates in Maxworthy (1991), $Fr_{\alpha,\min}$ was at a maximum at $\alpha = 0°$ and decreased as $\alpha \to 90°$. Similar behaviour is found in figure 8 where bubbles of $\lambda \leqslant 1.1$ display maximum $Fr_{\alpha,\min}$ values at either $\alpha = 5°$ or $\alpha = 25°$ after which $Fr_{\alpha,\min}$ decreases as $\alpha \to 90°$. The differences between Maxworthy's (1991) results and the current results at small α may be attributed to the effects of drying and the confining nature of the tube, especially for large λ. The dependence of $Fr_{\alpha,\min}$ on α in the acrylic tube system is similar to that observed for glass except the effects of drying are more severe and produce near-zero $Fr_{\alpha,\min}$ values for $\lambda \leqslant 1.1$ at $\alpha = 5°$.

3.5. *Pressure difference analysis*

The minimum pressure differences, $\Delta P_{\min}$, measured in the glass tube experiments are presented in dimensionless form in figure 9 as a function of bubble size and inclination angle. The pressures have been scaled with an inertial pressure scale such that $\Delta P_{\min} = \Delta P^*_{\min}/\rho U^2$. In figure 9(*a*) a nonlinear dependence of $\Delta P_{\min}$ on bubble size is observed. While there is little differentiation in the $\Delta P_{\min}$ values for $\lambda \leqslant 0.9$, as λ increases beyond $\lambda = 1$, a definite α dependence is observed with the highest values associated with the vertical tube ($\alpha = 90°$). It was shown in figure 7 that the minimum flow required for suspension was essentially constant for $\lambda \geqslant 1$. In figure 9(*a*) we see that $\Delta P_{\min}$ continues to increase with λ despite the fixed flow rates. This may be accounted for by recalling that for $\lambda \geqslant 1$, the cross-sectional profile of the bubble is fixed and the bubble simply elongates as λ increases (figures 2 and 4). Although the flow required to suspend the bubbles is the same, the liquid gap region between the bubble and the lower tube wall is longer for the larger bubbles. Hence, for a fixed flow, a higher driving pressure would be required for the bulk flow to completely traverse the longer bubble. The bubble might be said to act as a constriction in the tube and as this constriction lengthens, the driving pressure must increase to maintain a fixed flow rate. The overall effect of the bubble on the driving pressures would be dependent upon the combined effects of the shrinking gap width (for $\lambda < 1$), increasing bubble length, and the replacement of the no-slip

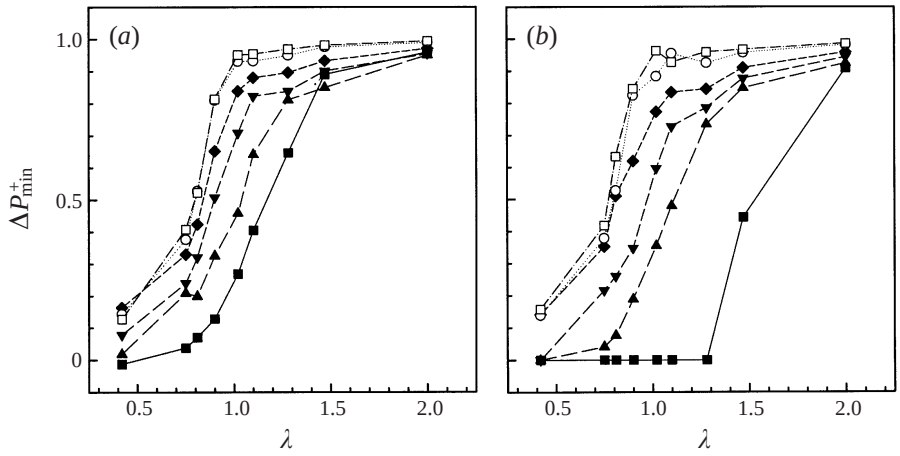

FIGURE 10. $\Delta P^{+}_{\min}$ vs. λ for bubbles in (*a*) glass and (*b*) acrylic tubes: ■, $\alpha = 5°$; ▲, $\alpha = 25°$; ▼, $\alpha = 45°$; ◆, $\alpha = 65°$; ○, $\alpha = 85°$; □, $\alpha = 90°$.

boundary with a stress-free interface. The continued increase of $\Delta P_{\min}$ for $\lambda > 1$ shown in figure 9(*a*) demonstrates the minimal effect of the boundary replacement. The dependence of the pressure differences on bubble size for the acrylic tube experiments is found to be similar to that depicted in figure 9(*a*) for the glass tube experiments.

The inclination angle dependence of the scaled pressure differences for the glass tube experiments is presented in figure 9(*b*), which indicates that the lowest and highest pressure differences are associated with bubbles in tubes inclined to 45° and 90°, respectively. A rather symmetric dependence of $\Delta P_{\min}$ is observed about $\alpha \sim 45°$, especially for large λ. Again, the general dependence of scaled pressures on inclination angles in acrylic tubes was determined to be similar to that observed in figure 9(*b*) for glass tube experiments.

In addition to analysing the overall pressure differences associated with the suspended bubbles, we also examine the added pressure due to the presence of the bubble, i.e. $\Delta P^{+*}_{\min}$. Prior to this, characteristic relationships of pressure difference versus flow rate are constructed for flows in the acrylic and glass tubes without bubbles present. The linear results yield that for the acrylic tube $\Delta P^{*}(\mathrm{cm\,H_2O}) = 2.43 \times 10^{-3}\, Q^{*}\,(\mathrm{cm^3\,min^{-1}})$ and for the glass tube $\Delta P^{*}(\mathrm{cm\,H_2O}) = 3.96 \times 10^{-3}\, Q^{*}(\mathrm{cm^3\,min^{-1}})$. As a check of the realistic nature of our flow apparatus, similar relationships are derived using Poiseuille flow theory with estimates of the viscosity and density of the bulk fluid. These calculations yield proportionality coefficients of 2.94×10^{-3} and 4.06×10^{-3} for the acrylic and glass tubes, respectively. The similarity of the experimental and theoretical relationships provides assurance that the experimental apparatus is indeed producing steady, laminar flow as designed.

For each experiment, the measured suspension flow rate, $Q^{*}_{\min}$, is used to determine ΔP^{*}_{Q} which is the pressure difference required to generate $Q^{*}_{\min}$ through the tube with no bubble present. Upon subtraction of ΔP^{*}_{Q} from $\Delta P^{*}_{\min}$, a measure of the added pressure difference due to the bubble, $\Delta P^{+*}_{\min}$, is obtained. Figure 10 presents the behaviour of the dimensionless added pressure difference, $\Delta P^{+}_{\min}$, as a function of λ and α where $\Delta P^{+}_{\min} = \Delta P^{+*}_{\min}/\Delta P^{*}_{\min}$. For both tube materials, a sigmoidal relationship is found between $\Delta P^{+}_{\min}$ and λ for all α. At a fixed inclination angle, an increase in bubble size results in an increased portion of the measured pressure that is attributable to

the presence of the bubble. For small bubbles requiring higher flows for suspension, the measured pressure differences are derived primarily from the bulk flow, indicating that a small bubble has minor effect on the flow mechanics. Larger bubbles, however, have a much greater effect on the flow mechanics as indicated in figure 10 in which the measured pressure differences for the largest bubbles are primarily attributable to the presence of the bubbles. For a fixed bubble size, an increase in the inclination angle also results in an increase in the scaled added pressure difference, indicating that suspended bubbles have a greater effect on the fluid flow in tubes oriented closer to the vertical position ($\alpha = 90°$).

The effects of changing the tube material may be seen in a direct comparison of the two plots in figure 10 where for most α and λ, the portion of the measured pressure due to the presence of the bubble is lower in the acrylic tubes, i.e. a suspended bubble in an acrylic tube has a smaller effect on the fluid mechanics. For a fixed bubble size and tube inclination, a bubble in an acrylic tube would tend to be easier to suspend due to the stronger contact forces in the air/water/acrylic system. The differences in scaled pressures between the two systems are observed to disappear as $\alpha \to 90°$ where the contact forces are absent.

4. Conclusions

We have presented here an investigation into the underlying mechanical and physicochemical phenomena of a gas bubble suspended within a liquid flow. The primary forces found to be governing overall bubble behaviour are the inertial forces derived from the flow, the buoyancy force of the bubble, and the contact forces for bubbles which dry the tube wall. The manipulation of the inclination angle, bubble size, and tube material modifies these forces in a very complex interdependent manner. A great deal of this complexity is attributable to the elaborate nature of the three-dimensional bubble geometry upon which the governing forces act.

The results of the current experiments demonstrate the effects a bubble may have if infused into a liquid flow in which buoyancy effects are important. In order to maintain a fixed flow rate, as may be required in many industrial processes, a significant increase in the driving pressure may be required with a bubble present. The magnitude of the pressure increases would be dependent upon the volume of gas infused (λ) and the inclination of the tube (α). As shown in figure 10, smaller bubbles would tend to have a lesser effect than larger bubbles. Should a mechanical system be limited to a certain driving pressure range, system performance could be severely reduced should an appropriately sized volume of air enter the system. For example, within the human vasculature, a bubble lodged in a major vessel may result in a drastic increase in the work of the heart in order to maintain adequate blood flow through the obstructed vessel.

The possibility of a gas bubble drying onto a tube surface may also have profound implications for the operation of a fluid system. The current results show that should a bubble dry to a surface, it may remain lodged for a range of bulk flows dependent upon bubble size and tube inclination (figures 2, 3, 5 and 6). The ability of dried bubbles to withstand bulk flow modifications and remain stationary is found to be material dependent and attributed to contact mechanics and gas–liquid interfacial deformation. Should a fluid system involve a pulsatile flow, a bubble may remain lodged over the entire pulsatile period if neither a low enough nor high enough bulk flow is reached. Similarly, if a fluid system has a maximum flow limit, a dried bubble may remain lodged if the maximum allowable flow is not

high enough to generate sufficient forces to dislodge the bubble. The exact geometry a stationary bubble will exhibit would be strongly dependent upon the mechanics of the nearby flow field as was demonstrated by Feng & Basaran (1994). While Addlesee & Cornwell (1997) report the presence of a thin liquid film between a rising bubble and an inclined plate, the occurrence of drying in the present investigation demonstrates the impact of tube geometry and material properties on interfacial mechanics.

As demonstrated in this investigation, contact angle hysteresis, when defined as $\phi_a - \phi_r$, is not a suitable sole indicator of the importance of contact forces. Although both material systems reveal similar contact angle hysteresis values (table 1), bubbles in the acrylic tube system are suspended over wider flow ranges than equally sized bubbles in glass tubes (figures 5 and 6). Therefore, the magnitudes of the advancing and receding contact angles are determined to play the primary role in governing the suspension of dried bubbles over ranges of flows.

To demonstrate the complex interdependence observed in this investigation, we provide a brief discussion of how the simple modification of bubble size directly affects all of the forces acting on the bubble. Initially, an increase in the size of a non-drying bubble within a vertical tube would seem to require an increase in the bulk flow in order to counteract the increased buoyancy force. The increasing bubble size, however, also results in the modification of the flow-derived inertial and viscous forces which may require further flow modifications to maintain suspension of the bubble. Also associated with the larger bubble is the possible modification of the local fluid mechanics in the vicinity of the gas–liquid interface. Changes in the flow field may include phenomena such as vortex formation, vortex shedding, or turbulence which may modify bubble shape which in turn will directly affect the flow field. To further complicate matters, should the tube be inclined off the vertical, a radial buoyancy component will tend to deform the bubble in an asymmetric manner which will affect the flow field and the flow derived forces. Lastly, if the bubble has dried the tube wall, an increase in bubble size will directly affect the magnitude of the contact forces through the modification of the size of the contact perimeter.

Due to the demonstrated interdependent complexity of the mechanical problem of interest, the application of simple or relatively straightforward force balance analyses in order to develop a representative model is extremely difficult. It is the complex three-dimensional geometry which acts as the limiting step. Even standard assumptions about the bubble geometry, such as the bubble being a spherically capped elongating cylinder, are found to be severely inadequate. The lack of the ability to adequately describe the bubble geometry, surface area, and contact perimeter as functions of bubble volume and inclination angle acts as a major impediment to scaling out an appropriate force balance.

Our demonstration of the complex interaction of the relevant forces in the current flow problem correlates well with previous gas bubble and liquid drop investigations. Although certain past investigators have recognized the possible importance of contact mechanics, none have put forth a quantitative analysis. This investigation directly demonstrates the critical importance of these material-dependent interactions on gas bubbles suspended in inclined tubes containing liquid flow.

The authors would like to thank Professor Michael J. Miksis for his valuable input and advice throughout this project. Support for the current investigation has been provided by the Whitaker Foundation and NIH grant R01 HL60230.

REFERENCES

Addlesee, A. J. & Cornwell, K. 1997 Liquid film thickness above a bubble rising under an inclined plate. *Chem. Engng Res. Des.* **75**, 663–667.

Brenner, H. 1970 Pressure drop due to the motion of neutrally buoyant particles in duct flows. *J. Fluid Mech.* **43**, 641–660.

Brenner, H. 1971 Pressure drop due to the motion of neutrally buoyant particles in duct flows. II. Spherical droplets and bubbles. *Ind. Engng Chem. Fundam.* **10**, 537–543.

Bretherton, F. P. 1961 The motion of long bubbles in tubes. *J. Fluid Mech.* **10**, 166–188.

Chang, H. K., Weber, M. E., Thomson, J. & Martin, R. R. 1981 Hydrodynamic features of pulmonary air embolism: a model study. *J. Appl. Physiol.* **51** (4), 1002–1008.

Dimitrakopoulos, P. & Higdon, J. J. L. 1997 Displacement of fluid droplets from solid surfaces in low-Reynolds number shear flows. *J. Fluid Mech.* **336**, 351–378.

Durbin, P. A. 1988 Free-streamline analysis of deformation and dislodging by wind force of drops on a surface. *Phys. Fluids* **31**, 43–48.

Dussan V., E. B. 1985 On the ability of drops or bubbles to stick to non-horizontal surfaces of solids. Part 2. Small drops or bubbles having contact angles of arbitrary size. *J. Fluid Mech.* **151**, 1–20.

Dussan V., E. B. 1987 On the ability of drops or bubbles to stick to non-horizontal surfaces of solids. Part 3. The influences of motion of the surrounding fluid on dislodging drops. *J. Fluid Mech.* **174**, 381–397.

Dussan V., E. B. & Chow, R. T.-P. 1983 On the ability of drops or bubbles to stick to non-horizontal surfaces or solids. *J. Fluid Mech.* **275**, 351–378.

Extrand, C. W. 1998 A thermodynamic model for contact angle hystersis. *J. Colloid Interface Sci.* **207**, 11–19.

Extrand, C. W. & Kumagai, Y. 1987 An experimental study of contact angle hystersis. *J. Colloid Interface Sci.* **191**, 378–383.

Fan, L. & Tsuchiya, K. 1990 *Bubble Wake Dynamics in Liquids and Liquid–Solid Suspensions.* Butterworth–Heinemann.

Feng, J. Q. & Basaran, O. A. 1994 Shear flow over a translationally symmetric cylindrical bubble pinned on a slot in a plane wall. *J. Fluid Mech.* **275**, 351–378.

Good R. J. & Koo, M. N. 1979 The effect of drop size on contact angle. *J. Colloid Interface Sci.* **71**, 283–292.

Hetsroni, G., Haber, S. & Wacholder, E. 1970 The flow fields in and around a droplet moving axially within a tube. *J. Fluid Mech.* **41**, 689–705.

Iliev, S. D. 1997 Static drops on an inclined plane: Equilibrium modeling and numerical analysis. *J. Colloid Interface Sci.* **194**, 287–300.

Kojima, E., Akehata, T. & Shirai, T. 1975 Behavior of single air bubbles held stationary in downward flows. *J. Chem. Engng Japan* **8**, 108–113.

Li, X. & Pozrikidis, C. 1996 Shear flow over a liquid drop adhering to a solid surface. *J. Fluid Mech.* **307**, 167–190.

Maneri, C. C. & Zuber, N. 1974 An experimental study of plane bubbles rising at inclination. *Intl J. Multiphase Flow* **1**, 623–645.

Marmur, A. 1997 Line tension and the intrinsic contact angle in solid-liquid-fluid systems. *J. Colloid Interface Sci.* **186**, 462–466.

Maxworthy, T. 1991 Bubble rise under an inclined plate. *J. Fluid Mech.* **229**, 659–673.

Moo-Young, M., Fulford, G. & Cheyne, I. 1971 Bubble motion studies in a countercurrent flow apparatus. *Ind. Engng Chem. Fundam.* **10**, 157–160.

Olbricht, W. L. & Leal, L. G. 1982 The creeping motion of liquid drops through a circular tube of comparable diameter: the effect of density differences between the fluids. *J. Fluid Mech.* **115**, 187–216.

Reinelt, D. A. 1987 The rate at which a long bubble rises in a vertical tube. *J. Fluid Mech.* **175**, 557–565.

Spelt, J. K., Li, D. & Neumann, A. W. 1992 The equation of state approach to interfacial tensions. In *Modern Approaches to Wettability* (ed. M. E. Schrader & G. T. Loeb), pp. 101–141. Plenum.

Tsao, H.-K. & Koch, D. L. 1997 Observations of high Reynolds number bubbles interacting with a rigid wall. *Phys. Fluids* **9**, 44–56.

White, E. T. & Beardmore, R. H. 1962 The velocity of single cylindrical air bubbles through liquids contained in vertical tubes. *Chem. Engng Sci.* **17**, 351–361.

Zukoski, E. E. 1966 Influence of viscosity, surface tension, and inclination angle on motion of long bubbles in closed tubes. *J. Fluid Mech.* **25**, 821–835.